




In the format provided by the authors and unedited.

Electrical detection of single magnetic skyrmions in metallic multilayers at room temperature

Davide Maccariello , **William Legrand** , **Nicolas Reyren** , **Karin Garcia**, **Karim Bouzehouane**, **Sophie Collin**, **Vincent Cros*** and **Albert Fert**

Unité Mixte de Physique, CNRS, Thales, Univ. Paris-Sud, Université Paris-Saclay, Palaiseau, France. *e-mail: vincent.cros@cnrs-thales.fr

Supplementary Information

Room temperature electrical detection of single magnetic skyrmion in magnetic multilayers

Davide Maccariello, William Legrand, Nicolas Reyren, Karin Garcia, Karim Bouzehouane, Sophie Collin, Vincent Cros*, and Albert Fert

1 Determination of the skyrmion size from Scanning Transmission X-ray Microscopy

The purpose here is to explain how we estimated the skyrmion diameter from Scanning Transmission X-ray Microscopy (STXM) images obtained on the multilayer with composition Ta(5)|Pt(10)|[Co(0.8)|Ir(1)|Pt(1)]₂₀|Pt(x) (in parentheses are given the thicknesses in nanometers), deposited on 200-nm-thick Si₃N₄ membranes. As described in details hereafter, from the raw images, we first produce a map of the magnetization (convolution of real skyrmion with the x-ray beam). Then this profile of the magnetization is compared to several simulated profiles in order to determine the skyrmion diameters from the best matching (see Fig.S1b).

STXM performed with circularly polarized light normal to the sample plane provides a direct measurement of the out-of-plane magnetization m_z . However, because the typical skyrmion size in the sub-100nm range is hence comparable to the beam size (*e.g.*, its full width at half maximum, FWHM), the determination of the actual skyrmion size requires a careful analysis described just after. Moreover, at the PolLux beamline (Swiss Light Source), the polarization is achieved by a bending magnet with a polarization level of about 70%, which furthermore can vary from one polarization to the other. Here we show how we recover a signal proportional to m_z (convoluted by the beam shape).

We assume that the transmitted intensity is $I_{\text{pol}} = I_{\text{pol}}^0 \exp(-\mu_{\text{pol}}t)$, pol being the effective polarization p or m corresponding to the light polarization σ_+ and σ_- , μ_{pol} the absorption coefficient, t the thickness of the materials, and I_{pol}^0 the intensity of the beam through the membrane without magnetic materials. We hence first normalize the intensity map of each polarization to the mean intensity through the membrane, and then take the log of the result to get a map of the local absorption. The difference of the absorption maps $\mu_p - \mu_m$, which proportional to m_z convoluted with the beam shape, is plotted in Supplementary Fig.S1a. The values of $\mu_p - \mu_m$ are normalized to -1 at the level corresponding to $m_z = -1$.

The size of the beam is calculated according to the opening of slits in the optics, as well as to the quality of the zone plate (the Fresnel lens focusing the x-rays). It can also be evaluated experimentally considering focus scans at edges of patterned structures. We estimate the effective FWHM of the beam to be about 100 ± 10 nm in our experimental conditions, about 25 nm larger than the calculated size. We assume a Gaussian shape of the beam. It is needed to make another assumption concerning the shape of the magnetization in the skyrmion, for which we used the formula of the main text, $m_z(r) = -\cos\{2\pi - 2\arctan(\exp(\frac{r-r_0}{\Delta})) - 2\arctan(\exp(\frac{r+r_0}{\Delta}))\}$, where $\Delta = 10$ nm is the domain wall width and r_0 is the radius of the skyrmion (taken from the center of the structure to the center of the domain wall). Following these hypotheses, we simulate the expected experimental profile for skyrmions of variable diameters. In Supplementary Fig.S1b, the experimental profiles (average of three 20 nm-wide

*Corresponding author: vincent.cros@cnsr-thales.fr

lines crossing the skyrmion core) is compared to the simulated profiles (averaged over the same width) for various values of r_0 , 20 nm, 30 to 50 nm by 2 nm steps, and 60 nm. We note that the precise value of Δ does not change appreciably the simulated profiles.

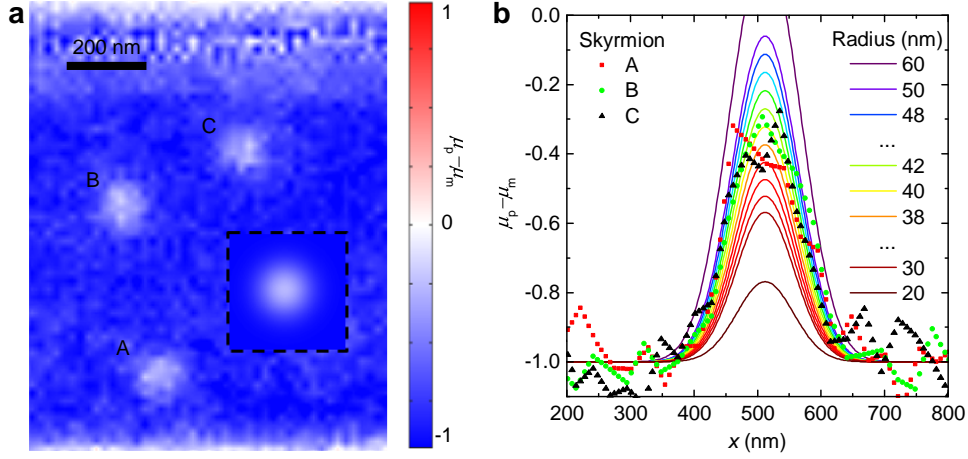
Finally, comparing the results of the series of simulations with the experimental data, we conclude from the best matching simulated curve with the experimental ones that the skyrmion diameter is 80 ± 8 nm.

2 Anomalous Hall effect as a probe of the out-of-plane magnetization

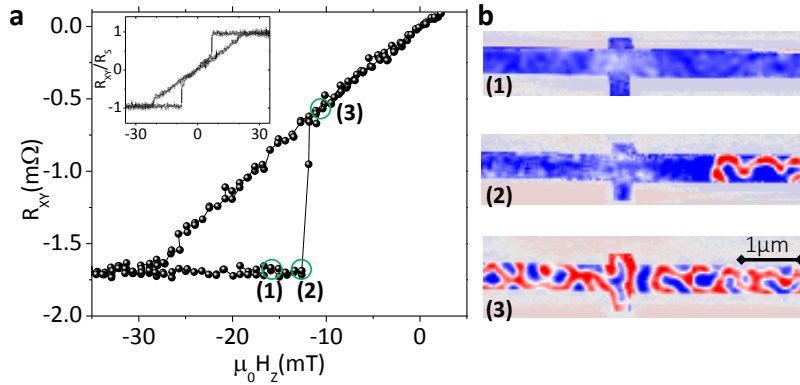
The efficiency of the electrical probe of the local magnetic configuration in the Hall cross area is shown in Supplementary Fig.S2: The transverse resistance R_{xy} of a track-shaped Pt(10)|[Pt(1)|Co(0.6)|Al₂O₃(1)]₅Pt(x) sample (a different one than the main text) is plotted as a function of H_{\perp} . Starting from large negative field, the uniform magnetic state is assessed by both the MFM image and the saturation of the Hall resistance. The state is preserved when the absolute value of the field is decreased (point (1), still $H_{\perp} < 0$). If the magnetic field is set at the value of the point (2), the Hall resistance remains constant while the MFM phase map shows the onset of worm-like magnetic domains in the track, still about $1.5 \mu\text{m}$ away from the center of Hall cross. Only modifications of the magnetic configuration in an effective region of Hall cross with lateral size of the order of the channel width contribute to the Hall resistivity changes [1, 2]. As shown in Fig.S 2 (point (3)), the variation of R_{xy} can be observed only when a magnetic domain approaches or is nucleated in the Hall cross area, (point (3)): After a sudden change of R_{xy} associated with the appearance of a first reversed magnetic domain in the Hall cross area, the transverse resistance then smoothly evolves with the size of magnetic domains growing in the Hall cross.

References

- [1] Thiaville, A., Belliard, L., Majer, D., Zeldov, E. & Miltat, J. Measurement of the stray field emanating from magnetic force microscope tips by Hall effect microsensors. *Journal of Applied Physics* **82**, 3182–3191 (1997).
- [2] Guillou, H., Kent, A., Stupian, G. W., Leung, M. S. Geometries for high spatial resolution Hall probes. *Journal of Applied Physics* **93**, 2746–2751 (2003).



Supplementary Fig.S 1: **Estimation of the skyrmion diameter.** **a**, Map of the absorption difference $\mu_p - \mu_m$, proportional to the out-of-plane magnetization m_z . Inserted in the STXM map, surrounded by dashed lines, a simulated image of a skyrmion convoluted with a Gaussian beam of 100 nm FWHM (using $\Delta = 10$ nm). **b**, Comparison between simulated profiles of skyrmions with various diameters with the three skyrmions profile in panel a.



Supplementary Fig.S 2: **Hall resistance vs. magnetic configuration in the Hall cross.** **a**, Hall resistance and nucleation of magnetic domain in a selected region of out-of-plane field hysteresis loop. In the inset we show the full hysteresis loop of R_{xy} normalized to the value in saturation. The MFM phase maps in **b**, shows that the transverse resistance R_{xy} is constant (point (1) and (2)) until magnetic domains enter the Hall cross. In (2) the MFM image evidences the nucleation of worm domains in the track far from the Hall cross. R_{xy} exhibits variations only when the the magnetization evolution interests the Hall cross area (3).